WILEY-VCH

Dynamically Reconfigurable Short-Term Synapse with Millivolt Stimulus Resolution Based on Organic Electrochemical Transistors

*Haifeng Ling, Naixiang Wang, Anneng Yang, Yanghui Liu, Jiajun Song and Feng Yan**

Dr. H. Ling, Dr. N. Wang, A. Yang, J. Song, Prof. F. Yan
Department of Applied Physics, Hong Kong Polytechnic University, Hong Kong SAR, China
E-mail: apafyan@polyu.edu.hk

Dr. Y. Liu
School of Materials, Sun Yat-sen University, Guangzhou 510275, China

Keywords: Artificial synapse, Short-term plasticity, OECT, Electrochemical doping, Conducting polymer,

Abstract.

Electrolyte-gated organic electrochemical transistors (OECTs) have been attractive for synaptic electronics owing to the ionic-electronic coupling, huge specific capacitance, physiological environmental compatibility and architectural flexibility. Here, we reported an identical spike-polarity method to realize the concomitance of excitatory and inhibitory short-term plasticity in unipolar poly(3,4-ethylenedioxythiophene)−poly(styrenesulphonate) (PEDOT:PSS) OECTs. Dynamical reconfiguration between the excitatory and inhibitory responses with multi-level and well-balanced synaptic strength is realized, without preforming operations or introducing additional modulation terminals. Owing to the distinctive volumetric capacitance of OECTs, the PEDOT:PSS synapse affords remarkable characteristics such as ultrahigh stimulus-resolution capability of 10 mV and ultralow power consumption of ~2 pJ/spike. Moreover, spatiotemporal correlated logics was realized. This work demonstrates on-demand manipulation of ionic dynamics for building synaptic elements with sophisticated functionalities at a single-device level.

1. Introduction

Brain inspired neuromorphic chips using microelectronic devices to emulate biological neural network functionalities, has emerged as hardware implementation of artificial intelligence.[1, 2] In a neural system, the communication between a pair of pre- and postsynaptic neurons is *via* the synapse. In this case, the realization of synaptic plasticity is regarded as the footstone for a neuromorphic system. Various electronic platforms have been developed to produce artificial synapses, mainly including two-terminal memristors and three-terminal thin-film transistors.[3, 4] Triggered by presynaptic voltage spikes, the resulting resistance state is defined as the connectivity strength between pre- and postsynaptic neurons in memristors,[5, 6] while the channel conductance represents the synaptic strength in transistors.[7-9] In biological synapses, the co-release of both glutamate and GABA neurotransmitters from a single axon terminal, rendering the strengthening and weakening of the synaptic connection, respectively. The concomitant and independently expressed excitatory and inhibitory postsynaptic responses are essential to a neural network.[10] A single artificial synapse capable of complete emulation of both excitatory and inhibitory activities, and especially their reconfiguration, is critical to building neuromorphic systems with desirable versatility and homeostatic plasticity.[11]

The concomitance of excitatory and inhibitory plasticities and their dynamical reconfigurations have been well reproduced in two-terminal memristors by changing the polarity of the presynaptic voltage.[12, 13] However, the same implementations remain challenging in unipolar transistors because of the nonequilibrium mobile carrier concentration. Recently, this challenge has been addressed in 2D material-based transistors by introducing an additional control terminal. Owing to the ambipolar conductance of graphene or molybdenum disulfide (MoS_2), both behaviors of excitatory postsynaptic current (EPSC) and inhibitory postsynaptic current (IPSC) could be triggered by changing the polarity at the dual-gate terminals,[14] or using positive/negative gate voltage combining external light terminal.[15-17]. Although impressive accomplishments have been made, there are always limitations on the

selection of ambipolar materials, and additional control terminals would increase the complexity the circuit design. Consequently, unipolar synaptic transistors with in-situ modulated excitatory and inhibitory plasticity are highly desirable. Moreover, these achievements were based on field-effect transistors (FETs), in which too high presynaptic voltage (tens of volts) is always required to overcome the inherent limitation of dielectric thickness-dependent capacitance (nF/cm^2). [11, 15, 18, 19]

Electrolyte-gated transistor (EGT) represents a hybrid ionic/electronic conduction device capable of efficient capacitance coupling, biocompatibility and flexible architecture.[20] Typically, two major categories of EGTs have been employed for synaptic electronics depending on the permeability of semiconductor channel to the ions of the electrolyte.[21, 22] The impermeable one is often known as electrical double layer transistors (EDLTs), for which ion accumulation related EDL capacitance (μF/cm^2) will modulate the channel conductance.[23-25] The other one is the organic electrochemical transistor (OECT), that is based on electrochemical doping/de-doping processes upon bulk injection of ionic species to the redox-active channel materials.[26] One unique feature of synaptic OECTs is the high volumetric capacitance that allows the channel conductance to be precisely manipulated in a narrow voltage range (< 1 V).[27] Furthermore, the electrolyte, either liquid or solid, plays the role of a global regulation medium in analogy with the neural environment. This feature facilitates the integration of multi-input/output interconnected architectures,[28, 29] endowing synaptic OECTs a significant advantage in mimicking spatiotemporally correlated functions.[30, 31] In nervous system, short-term plasticity (STP) supports a variety of computation tasks including the transmission, encoding, and filtering of the neural signal. Despite the advances in implementing short-term inhibitory synapse with OECTs,[26, 28] the concomitant excitatory synapse remains absent. Compared to the recent developments in EDLTs for mimicking biological synapse, the co-existence and especially the dynamical reconfiguration of excitatory and inhibitory plasticity has been rarely demonstrated in existing OECTs.

In this study, we reported a facile method of in situ regulation for the concomitant and reconfigurable inhibitory and excitatory plasticity in unipolar PEDOT:PSS OECTs. Both short-term facilitation and depression of the synaptic strength could be mimicked by controlling the doping degree in PEDOT:PSS through a single gate below 1 V. Spike amplitude, duration and rate-dependent synaptic plasticities were successfully emulated in excitatory and inhibitory modes, respectively. Based on the concomitant and independently expressed synaptic activities, dynamical and balanced reconfiguration between excitatory and inhibitory response were realized owing to the rapid electrochemical doping process (~0.4 ms). Our work highlights the potential of unipolar OECT-based neuromorphic architecture to perform versatile functions for information processing.

2. Results and Discussion

2.1. Design of Synaptic OECTs

Figure 1a shows the schematic diagram of the PEDOT:PSS OECT. The PBS electrolyte with Pt terminal is regarded as the presynaptic neuron to receive the input signal, and the PEDOT:PSS channel together with the source–drain electrodes serves as the postsynaptic neuron that transmits the output signal, i.e., the postsynaptic current (PSC) in the form of the source–drain current (I_D). When a positive voltage (V_{Pre} with amplitude V_P, duration t_d) is applied at the Pt gate, cations (predominantly Na^+) in the PBS electrolyte are pushed to penetrate into the PEDOT:PSS channel and de-dope PEDOT from PSS. The initial highly conductive state (i.e., oxidized state) of PEDOT:PSS changes gradually to insulating neutral state (i.e., reduced state).[32, 33] The reversibility of doping/de-doping reactions makes the reversible modulation of channel conductance possible. As shown in **Figure 1b** and **1c**, I_D decreased with the increase of gate voltage, a maximum current on-off ratio of ~ 2.2×10^2 was obtained for the 1 uM PBS-gated OECT device. The appearance of hysteresis window during the forward and backward gate sweeping indicated slow kinetics of ionic movement in the

electrolyte, demonstrating a dependence of the channel conductance on the history of input stimuli. The gate–source current (I_G) was much lower than the I_D value (**Figure S1**), that was key to ensuring an efficient gate-channel coupling. Additionally, the transconductance (g_m) exhibited a convex shape with the peak value of 0.41 mS at V_G= 0.5 ± 0.01 V. This non-monotonic transconductance is the unique characteristic of OECTs, which is distinctively different from previously demonstrated synaptic transistors based on charge-trapping and EDL mechanisms.[18, 34] In this case, V_G= 0.5 V was selected as the presynaptic spike V_P, and V_{Pre}= 0 and 0.8 V were denoted as the input baseline, respectively (see supplementary materials for the selection details). **Figure 1d** shows the spike stressing stability of the synaptic OECTs. Continuous V_{Pre} pulses of 0 V and 0.8 V (t_d=10 ms, 100% duty cycle) created strong oxidized and reduced states of the PEDOT:PSS channel, respectively. The two conductance states were well maintained over 4×10^3 pulse stimuli, that would help the mimicking of stable resting states.

2.2. Concomitant and Independently Expressed Plasticity

Figure 2 shows the representative and independently expressed STP behaviors. With the baseline of V_{Pre}= 0 V, when a positive excitation spike (V_P=0.5 V, t_d=10 ms) was applied as the input signal, the PSC showed a sudden decay from 208.6 to 194.7 uA (**Figure 2a**). Once the V_P was removed, the PSC gradually recovered to its initial value. This process resulted a negative PSC change, that reproduced an IPSC process observed in biological inhibitory synapse. On the contrary, when the baseline bias was V_{Pre}= 0.8 V, the identical spike triggered a typical EPSC with a positive change from 5.9 to 13.9 uA, which matched the behavior of biological excitatory synapse (**Figure 2b**). The resulting inhibitory and excitatory dual modes in a single synaptic OECT can be explained from the different doping states in PEDOT:PSS channel. With the application of a positive presynaptic spike, cations are injected into the PEDOT:PSS film, drifting to the sites consisting of hole$^+$/PSS$^-$ pairs to compensate holes. PEDOT$^+$ is then

reduced from the conductive state to the insulating neutral state $PEDOT^0$. This reduction process electrically triggers an IPSC. After the presynaptic spike, cations gradually drift back out of the channel and PEDOT:PSS returns to its conductive state, making PSC gradually back to its original value. Differently, the excitatory phenomenon stem from the electrochemical oxidation of PEDOT:PSS channel under opposite direction of positive gate voltages. With the voltage offset (i.e., baseline bias) of 0.8 V, smaller amplitude of V_P (e.g., 0.5 V) would induce a relatively weak reduced state of the channel, thus triggering an EPSC response. Spike amplitude-dependent plasticity (SADP) is a typical postsynaptic activity of the STP effect. As exhibited in **Figure 2c** and **Figure S2a,b,** the peak value of IPSC decreased steadily with increasing amplitudes of presynaptic spikes from 205.5 uA for 0.1 V to 190.5 uA for 0.7 V, and the PSC variation (ΔPSC, defined as the value difference between peak and baseline of PSC) showed a significant linear relationship with V_P. In contrast, the EPSC tended to increase linearly as amplitudes of input pulses decreased from 6.9 uA for 0.7 V to 31.8 uA for 0.1 V. Specifically, the stimulus-resolution capability was determined to be 10 mV with a high signal-noise-ratio (SNR) of ~16 dB (**Figure 2d** and **Figure S3**), far below than that of biological synapses (55 mV) and those of previously reported synaptic transistors (**Table S1**). This is owing to the huge volumetric capacitance that endowing synaptic OECTs with ultrahigh coupling between ionic and electronic charges.[35] Postsynaptic activity was also performed in spike duration-dependent plasticity (SDDP) measurements as shown in **Figure 2e** and **Figure S2c,d**. For both IPSC and EPSC modes, the absolute value of ΔPSC increased synchronously with increasing t_d width, which was ascribed to much more cation injected/extractied in/from the PEDOT:PSS channel with longer duration time.[36] When the spike duration time reached 60 ms, ΔPSC tended to be saturated for the limited concentration of mobile cations in dilute electrolyte.[37] The energy consumption of our synaptic transistor could be reduced by varying the spike duration time and reading voltage (V_D), the lowest power dissipation was estimated to be ~2 pJ/spike (**Figure 2f**, see supplementary materials for calculation details), which is a

competitive value compared with other state-of-the-art organic synaptic transistors (**Table S2**). The high spiking current as well as the overall energy consumption, could be further reduced by adding reducing agents into PEDOT:PSS or by scaling the scaling the channel dimensions.[27, 38]

The temporal correlation between pre-and post-synapse is an essential STP effect for decoding temporal information in auditory or visual signals, since the synaptic facilitation or depression occurs and decays in a short-term scale after the specific activity. We emulated this dynamic process by applying a pair of pre-synaptic spikes (V_P = 0.5 V, t_d=10 ms) on Pt gate with an interspike interval time of Δt=50 ms. As shown in **Figure 3a**, two successive IPSC peaks were observed for the device operating in inhibitory mode. The peak value of the second peak (A2) was of ~194.9 uA and lower than that of the first peak (A1) of ~197.3 uA. Such behavior is analogous to the paired-pulse depression (PPD) behavior in biological synapses related to the more inhibitory neurotransmitters released at synaptic membrane. The PPD ratio (A2/A1), reflecting the information processing ability of inhibitory synaptic junction, was estimated to be ~0.98 in this case. Differently, two successive EPSC peaks appeared with a A2/A1 value of 1.13 for the device operating in excitatory mode (**Figure 3b**). This process represents a paired-pulse facilitation (PPF) characteristic in excitatory synaptic junction. To further quantify the temporal correlation, **Figure 3c** shows the PPD/PPF ratio plotted as a function of interval time Δt. With the increase of Δt, the PPD/PPF ratio increased/decreased exponentially to approach the value of 1 at a critical value of 300 ms. When the second spike was applied shortly after the first spike (Δt < 300 ms), a smaller fraction of injected cations induced by the first spike still reside in the channel and the total amount of the cations will get larger. Thus, the efficiency of ion-to-electron coupling was enhanced and the peak value of A2 was lower/higher than that of A1. In contrast, Δt > 300 ms was sufficient for the uptake of cations after the first spike, A1 can return to its original state. Beyond the critical Δt, the synaptic OECT operated at the information non-processing mode and the temporal correlations between

the two neurons were lost. PPD and PPF index curves were fitted with an exponential function (**Figure S4**), and the relaxation time τ_{PPD} and τ_{PPF} were estimated to be ~36.6 ms and ~33.1 ms, respectively. The obtained time scales are comparable to those of biological synapses. [34]

The temporal correlation effect was further explored by emulating the spike rate-dependent plasticity (SRDP). A stimulus trains consisting of 10 presynaptic spikes (t_d= 10 ms) with frequency ranged from 14.2 to 50 Hz were applied on Pt terminal. As depicted in **Figure 3d** and **3e** (33.3 Hz), continuous PSC peaks with gradual depressive/ facilitative conductance changes can be observed in response to the stimulus trains. To quantitatively compare the SRDP effect, we calculated the PSC gain (A10/A1) which is defined as the depression/facilitation ratio between the peak value of the tenth PSC peak (A10) and the first PSC peak (A1). **Figure 3f** shows that the gain value was proportional to high stimuli frequency as well as strong presynaptic spike strength ($|V_P-V_{Pre}|$), the lowest depression ratio and maximum facilitation ratio were 73% and 448%, respectively. The depression ratio can be further decreased by improving the stimuli frequency as well as the electrolyte concertation, and the lowest depression ratio can reach 48% (**Figure S5**). This frequency-dependent synaptic behavior could be used to mimic the dynamic filtering function for information transmission. As shown in **Figure 3g** and **3h**, high frequency input signals (50 Hz) can induce a strong suppression/potentiation effect to filter out the corresponding low/high frequency input signal, thus both low-pass/high-pass filtering functions can be implanted in a single synaptic device by modulating the synapse operation modes. We also found that pulse number has a great influence on the synaptic plasticity. As shown in **Figure 3i**, when the number of stimulus spikes increased, the PSC needed more time to recover to its base line, demonstrating a transition tendency from short-term memory to long-term memory. However, we note that nonvolatile memory is challenged to be implemented in this PEDOT:PSS-based OECTs. Due to the open and loose interconnected network of PSS chains,[39] cations drift quickly back out of the channel after the presynaptic spike. Hence, the conductance-state retention of the reduced PEDOT:PSS film

could not be maintained well. The memory effect could be further enhanced by inserting an ion barrier into the programming circuit (**Figure S6**).[27, 38]

2.3. Dynamic Reconfiguration and Multi-level Synaptic Strength

The working principles of inhibitory and excitatory dual modes are shown in **Figure S7**. Compared with previously reported synaptic transistors that requiring additional modulation terminals or initialization operation to trigger concomitant excitatory and inhibitory responses (**Table S1**), the OECT synapse shows the advantage of in-situ manipulation. All synaptic responses only depend on the signals inputted through the single Pt gate. However, it is difficult to implement different resting states quickly by simply changing the voltage offset in FET-based synapse. Generally, a higher preforming gate pulse was always required to set the synaptic device at a specific conductance states.[40, 41] Instead, different conductance states could be quickly achieved in ~ 0.4 ms for OECTs owing to the distinctive volumetric doping (see supplementary materials for the calculation details). We suggest that the proposed gate voltage-offset method could be generally adapted to unipolar synaptic OECTs. This identical spike-polarity operation allows flexible and dynamic reconfiguration between excitatory and inhibitory modes. As shown in **Figure 4a**, at a fixed baseline bias of V_{Pre}= 0.5 V, the PSC change presented a facilitative increasing trend when V_P was increased from 0.6 to 1.0 V, while the decrease of V_P from 0.4 to 0 V induced a depressive but balanced PSC variation. In this way, multi-level synapse strengths could be dynamically reconfigured in our OECTs (**Figure 4b**). The device can be reconfigured to be a strongly inhibitory, weakly excitatory/inhibitory, and strongly excitatory synapse, respectively. Hence, we could mimic the evolutionary process of both the inhibitory and excitatory synapses in a single artificial synapse.

2.4. Spatiotemporal Correlated Logics

Dendrite integration includes the integration of unsynchronized single events (temporal summation) and the simultaneous integration of single events occurring in different regions (spatial summation). **Figure 5a** shows the schematic diagram of the biological spatial summation from spatial isolated synaptic inputs. To mimic this spatial summation function, a multi-input to one-output transistor was proposed for artificial dendrite applications. Because of the spatial capacitance coupling, the transistor can process spatial−temporal input spikes received on the dendrites, and the channel current was deemed as an output. In the inhibitory measurements, presynaptic spikes (0.5 V, 10 ms) were applied on the dual in-plane Au gates (G1, G2) with the same electrode areas and one Pt gate (G3), respectively. The area of G3 is ≈27-fold larger than that of G1 and G2, thus G3 could be deemed as a modulatory terminal (Gm) to induce a stronger gating effect (**Figure S8**).[42] Three types of spatial summation have been implenmented from the different combinations of presynaptic inputs, that were analogous to the logic "AND", "YES_{G3}" and "OR" respectively. The input voltage of 0 and 0.5 V is defined as "0" and "1" respectively. As shown in **Figure 5b**, the binary inputs of "10", "01" and "11" were applied on G1 and G2, respectively. Only when input signals are "11," the IPSC was lower than the threshold value of 75 uA, which indicated the "AND" logic. As shown in **Figure 5c**, as long as input G3 was "1," the IPSC was lower than the threshold, which indicated the "YES_{G3}" logic. As shown in Figure **5d**, "OR" logic function was demonstrated when positive spikes were applied on the modulatory terminal (G3) synchronously with any one input spike of G1 and G2. These logic functions could also be realized under excitatory mode (**Figure S9**).

3. Conclusion

In summary, we have proposed an identical spike-polarity method to mimic the co-release of excitatory and inhibitory neurotransmitters on basis of electrochemical doping concept in a unipolar OECT. Typical STP effects including spike-amplitude, duration and rate-dependent

plasticity and temporal filtering are independently expressed under excitatory and inhibitory modes, repetitively. Our synaptic OECTs showed a stimulus-resolution capability down to 10 mV still holding high SNR of ~16 dB and low power consumption of *ca.* 2 pJ because of the large volumetric capacitance. Dynamical reconfiguration between the excitatory and inhibitory responses with multi-level connection strength was realized. Dendritic integrations in both synaptic modes were well mimicked. Combining the biocompatibility of conductive polymer to directly interface with physiological environment, the versatile electrolyte-gated synaptic OECTs hold promise in future neuroprosthetics.

4. Experimental Section

Materials: PEDOT:PSS (Clevios PH-500) was mixed with DMSO and glycerin (both with a volume ratio of 5%) to improve the conductivity and stability of channel films. In addition, the cross-linker GOPS was added to the above dispersion with a volume ratio of 1% to prohibit PEDOT:PSS dissolution. The electrolyte of phosphate buffered saline (PBS, Sigma-Aldrich Co., 0.1 M, pH=7.4) was diluted into different concentrations with deionized water, and defined as 1 uM to 1000 uM, respectively.

Device Fabrication: The devices were fabricated by using multilayer photolithography. Glass substrates were cleaned by chemical and plasma methods. The contact lines were defined by magnetron sputtering a 10 nm Cr and a 100 nm Au layer on top of prepatterned AZ5214 photoresist and then through a standard lift-off process. A second layer of AZ5214 photoresist was spin coated on the substrate with electrodes, and the channel window was opened by alignment photolithography. PEDOT:PSS was then spin coated on the patterned photoresist and annealed at 110 ℃ for 20 mins. After that, unwanted PEDOT:PSS with photoresist were removed by washing with acetone. At last, SU-8 photoresist was spin coated and patterned on the surface of the PEDOT:PSS film, acting as an insulating layer to protect the Au electrodes

from the aqueous electrolyte. The channel length (*L*) and width (*W*) of the devices were 30 and 60 μm, respectively.

Device Characterization: For gating, the fixed volume (10.0 μL) of droplet of dilute PBS (1 uM) was applied over the channel region from a microsyringe. One Pt wire was bent and penetrated into the PBS solution as the top gate electrode. To secure the repeatability, the Pt wire was washed by the deionized water several times and then dried by nitrogen gas. After that, the Pt wire was washed by the PBS solution several times before gating. The transistor characteristics and synaptic emulations were carried out using a semiconductor parameter analyzer (Keithley 4200 SCS).

Supporting Information
Supporting Information is available from the Wiley Online Library or from the author.

Acknowledgements
This work is financially supported by the Research Grants Council (RGC) of Hong Kong, China (project no. C5015-15G), and The Hong Kong Polytechnic University (project nos. 1-ZVGH, G-YBJ0, and 1-ZVK1).

Received: ((will be filled in by the editorial staff))
Revised: ((will be filled in by the editorial staff))
Published online: ((will be filled in by the editorial staff))

References

[1] Y. Kim, A. Chortos, W. Xu, Y. Liu, J. Y. Oh, D. Son, J. Kang, A. M. Foudeh, C. Zhu, Y. Lee, S. Niu, J. Liu, R. Pfattner, Z. Bao, T.-W. Lee, *Science* **2018**, *360*, 998.
[2] Y. van de Burgt, A. Melianas, S. T. Keene, G. Malliaras, A. Salleo, *Nat. Electron.* **2018**, *1*, 386.
[3] Z. Y. Wang, L. Y. Wang, M. Nagai, L. H. Xie, M. D. Yi, W. Huang, *Adv. Electron. Mater.* **2017**, *3*, 1600510.
[4] H. Han, H. Yu, H. Wei, J. Gong, W. Xu, *Small* **2019**, *0*, 1900695.
[5] W. Xu, H. Cho, Y.-H. Kim, Y.-T. Kim, C. Wolf, C.-G. Park, T.-W. Lee, *Adv. Mater.* **2016**, *28*, 5916.
[6] Y. Wang, Z. Lv, Q. Liao, H. Shan, J. Chen, Y. Zhou, L. Zhou, X. Chen, V. A. L. Roy, Z. Wang, Z. Xu, Y.-J. Zeng, S.-T. Han, *Adv. Mater.* **2018**, *30*, 1800327.
[7] L. Q. Zhu, C. J. Wan, L. Q. Guo, Y. Shi, Q. Wan, *Nat. Commun.* **2014**, *5*, 3158.
[8] Y. Zang, H. Shen, D. Huang, C. A. Di, D. Zhu, *Adv. Mater.* **2017**, *29*, 1606088.
[9] F. Alibart, S. Pleutin, D. Guérin, C. Novembre, S. Lenfant, K. Lmimouni, C. Gamrat, D. Vuillaume, *Adv. Funct. Mater.* **2010**, *20*, 330.
[10] H. Tian, W. Mi, H. Zhao, M. A. Mohammad, Y. Yang, P.-W. Chiu, T.-L. Ren, *Nanoscale* **2017**, *9*, 9275.
[11] H. Tian, X. Cao, Y. Xie, X. Yan, A. Kostelec, D. DiMarzio, C. Chang, L.-D. Zhao, W. Wu, J. Tice, J. J. Cha, J. Guo, H. Wang, *ACS Nano* **2017**, *11*, 7156.
[12] L. Wang, Z. Wang, W. Zhao, B. Hu, L. Xie, M. Yi, H. Ling, C. Zhang, Y. Chen, J. Lin, J. Zhu, W. Huang, *Adv. Electron. Mater.* **2017**, *3*, 1600244.
[13] C. Wu, T. W. Kim, H. Y. Choi, D. B. Strukov, J. J. Yang, *Nat. Commun.* **2017**, *8*, 752.
[14] H. Tian, W. Mi, X.-F. Wang, H. Zhao, Q.-Y. Xie, C. Li, Y.-X. Li, Y. Yang, T.-L. Ren, *Nano Lett.* **2015**, *15*, 8013.
[15] Q. Shuchao, W. Fengqiu, L. Yujie, W. Qing, W. Xinran, X. Yongbing, S. Yi, W. Xiaomu, Z. Rong, *2D Materials* **2017**, *4*, 035022.
[16] S. Wang, C. Chen, Z. Yu, Y. He, X. Chen, Q. Wan, Y. Shi, D. W. Zhang, H. Zhou, X. Wang, P. Zhou, *Adv. Mater.* **2019**, *31*, 1806227.
[17] J. Sun, S. Oh, Y. Choi, S. Seo, M. J. Oh, M. Lee, W. B. Lee, P. J. Yoo, J. H. Cho, J. H. Park, *Adv. Funct. Mater.* **2018**, *28*, 1804397.
[18] Y. Wang, Z. Lv, J. Chen, Z. Wang, Y. Zhou, L. Zhou, X. Chen, S.-T. Han, *Adv. Mater.* **2018**, *30*, 1802883.
[19] S. Dai, X. Wu, D. Liu, Y. Chu, K. Wang, B. Yang, J. Huang, *ACS Appl. Mater. Interfaces* **2018**, *10*, 21472.
[20] N. Wang, A. Yang, Y. Fu, Y. Li, F. Yan, *Acc. Chem. Res.* **2019**, *52*, 277.
[21] S. Jia, F. Ying, W. Qing, *J. Phys. D: Appl. Phys.* **2018**, *51*, 314004.
[22] Y. He, Y. Yang, S. Nie, R. Liu, Q. Wan, *J. Mater. Chem. C* **2018**, *6*, 5336.
[23] F. Yu, L. Q. Zhu, H. Xiao, W. T. Gao, Y. B. Guo, *Adv. Funct. Mater.* **2018**, *28*.
[24] W. Xu, S. Y. Min, H. Hwang, T. W. Lee, *Sci. Adv.* **2016**, *2*, 1501326.
[25] S. Dai, Y. Wang, J. Zhang, Y. Zhao, F. Xiao, D. Liu, T. Wang, J. Huang, *ACS Appl. Mater. Interfaces* **2018**, *10*, 39983.
[26] P. Gkoupidenis, N. Schaefer, B. Garlan, G. G. Malliaras, *Adv. Mater.* **2015**, *27*, 7176.
[27] Y. van de Burgt, E. Lubberman, E. J. Fuller, S. T. Keene, G. C. Faria, S. Agarwal, M. J. Marinella, A. Alec Talin, A. Salleo, *Nat. Mater.* **2017**, *16*, 414.
[28] P. Gkoupidenis, D. A. Koutsouras, G. G. Malliaras, *Nat. Commun.* **2017**, *8*, 15448.
[29] Y. Fu, L.-a. Kong, Y. Chen, J. Wang, C. Qian, Y. Yuan, J. Sun, Y. Gao, Q. Wan, *ACS Appl. Mater. Interfaces* **2018**, *10*, 26443.
[30] P. Gkoupidenis, D. A. Koutsouras, T. Lonjaret, J. A. Fairfield, G. G. Malliaras, *Sci. Rep.* **2016**, *6*, 27007.

[31] C. Qian, L.-a. Kong, J. Yang, Y. Gao, J. Sun, *Appl. Phys. Lett.* **2017**, *110*, 083302.
[32] J. Rivnay, S. Inal, A. Salleo, R. M. Owens, M. Berggren, G. G. Malliaras, *Nat. Rev. Mater.* **2018**, *3*, 17086.
[33] J. T. Friedlein, R. R. McLeod, J. Rivnay, *Org. Electron.* **2018**, *63*, 398.
[34] Y. H. Liu, L. Q. Zhu, P. Feng, Y. Shi, Q. Wan, *Adv. Mater.* **2015**, *27*, 5599.
[35] A. V. Volkov, K. Wijeratne, E. Mitraka, U. Ail, D. Zhao, K. Tybrandt, J. W. Andreasen, M. Berggren, X. Crispin, I. V. Zozoulenko, *Adv. Funct. Mater.* **2017**, *27*, 1700329.
[36] P. Gkoupidenis, N. Schaefer, X. Strakosas, J. A. Fairfield, G. G. Malliaras, *Appl. Phys. Lett.* **2015**, *107*, 263302.
[37] N. Wang, Y. Liu, Y. Fu, F. Yan, *ACS Appl. Mater. Interfaces* **2018**, *10*, 25834.
[38] S. T. Keene, A. Melianas, Y. v. d. Burgt, A. Salleo, *Adv. Electron. Mater.* **2019**, *5*, 1800686.
[39] S.-M. Kim, C.-H. Kim, Y. Kim, N. Kim, W.-J. Lee, E.-H. Lee, D. Kim, S. Park, K. Lee, J. Rivnay, M.-H. Yoon, *Nat. Commun.* **2018**, *9*, 3858.
[40] Y. Yao, X. Huang, S. Peng, D. Zhang, J. Shi, G. Yu, Q. Liu, Z. Jin, *Adv. Electron. Mater.* **2019**, *5*, 1800887.
[41] J.-Y. Mao, L. Hu, S.-R. Zhang, Y. Ren, J.-Q. Yang, L. Zhou, Y.-J. Zeng, Y. Zhou, S.-T. Han, *J. Mater. Chem. C* **2019**, *7*, 48.
[42] C. J. Wan, Y. H. Liu, P. Feng, W. Wang, L. Q. Zhu, Z. P. Liu, Y. Shi, Q. Wan, *Adv. Mater.* **2016**, *28*, 5878.

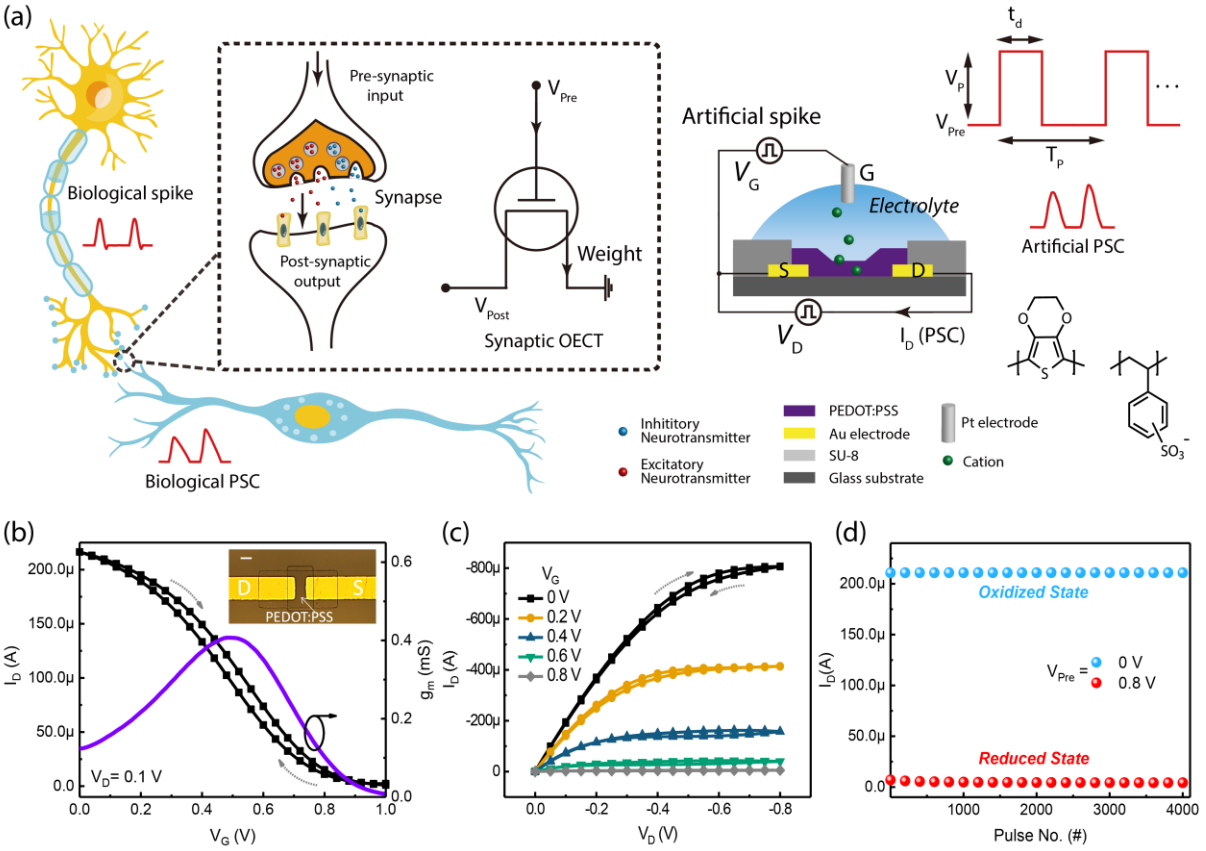

Figure 1. (a) Schematic demonstration of biological synapse, the sketch of a solution-gated PEODT:PSS OECT, and molecular structure of PEDOT:PSS. (b) Double sweeping of the transfer (I_D-V_G) characteristics and the associated transconductance (g_m) of the OECT. Inset is the optical micrograph of the OECT channel. Scale bar, 30 μm. (c) Double sweeping of the output (I_D-V_D) characteristics of the OECT. (d) Spike-stress stability of the OECT as a function of continuous presynaptic inputs (at V_D=0.1 V, t_d=10 ms, 100% duty cycle).

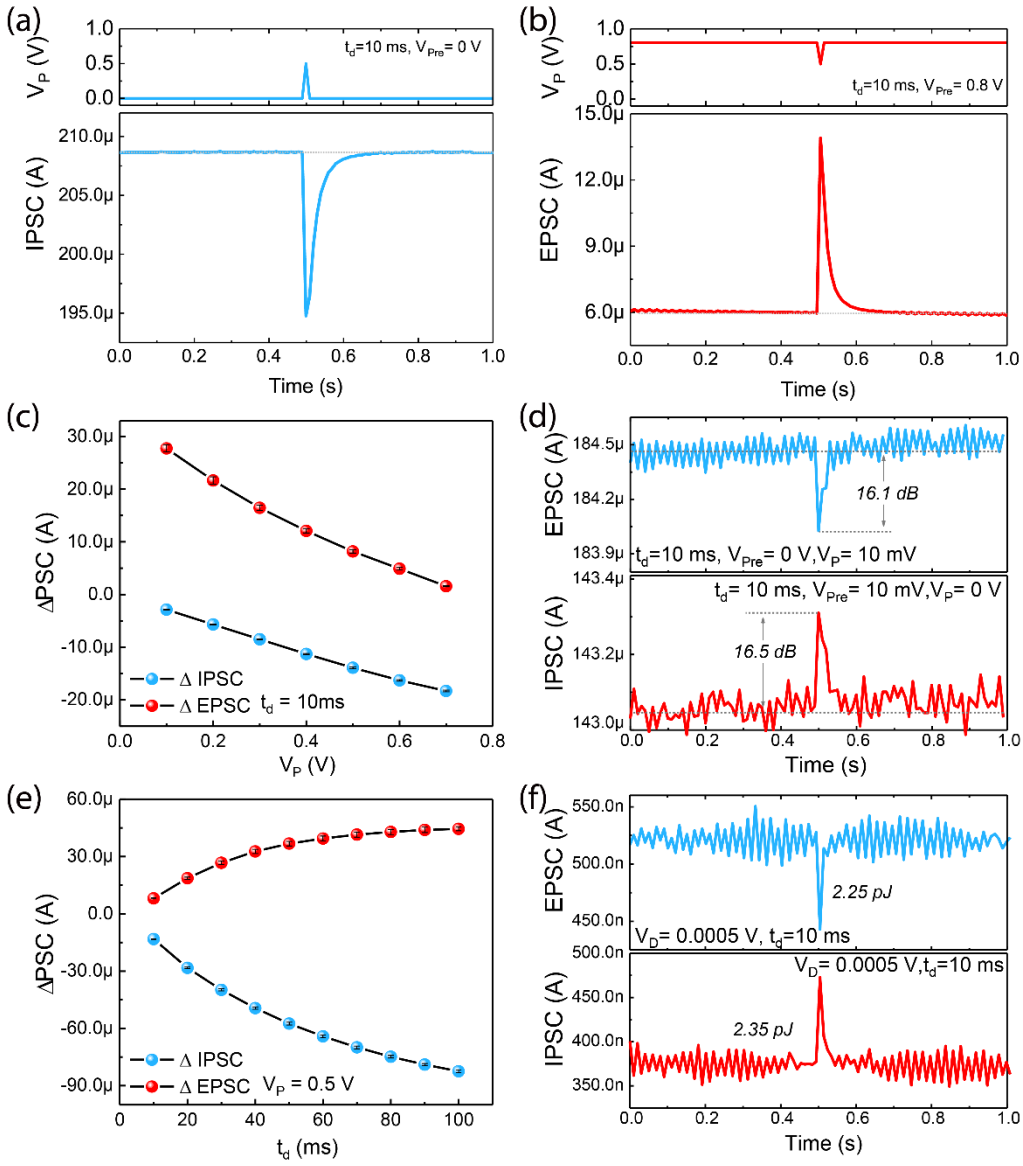

Figure 2. Typical postsynaptic current behaviors. (a) IPSC triggered by a presynaptic spike (V_{Pre} = 0 V, V_P=0.5 V, t_d=10 ms, V_D=0.1 V) . (b) EPSC triggered by a presynaptic spike (V_{Pre} = 0.8 V, V_P=0.5 V, t_d=10 ms, V_D=0.1 V). (c) Spike amplitude-dependent plasticity with a fixed spike duration of t_d=10 ms at V_{Pre} = 0 V (IPSC) and 0.8 V (EPSC), repectively. (d) The stimulus resolution and corresponding signal-to-noise ratio for IPSC (top) and EPSC (bottom). (e) Spike duration-dependent plasticity with a fixed spike amplitude of V_P=0.5 V at V_{Pre} = 0 V (IPSC) and 0.8 V (EPSC), repectively. (f) Energy consumption of per spike for IPSC (top, V_{Pre} = 0 V, V_P=0.3 V) and EPSC (bottom, V_{Pre} = 0.3 V, V_P=0 V). For (c) and (e), each point is collected from the average of five measured data, and the error bars are also plotted.

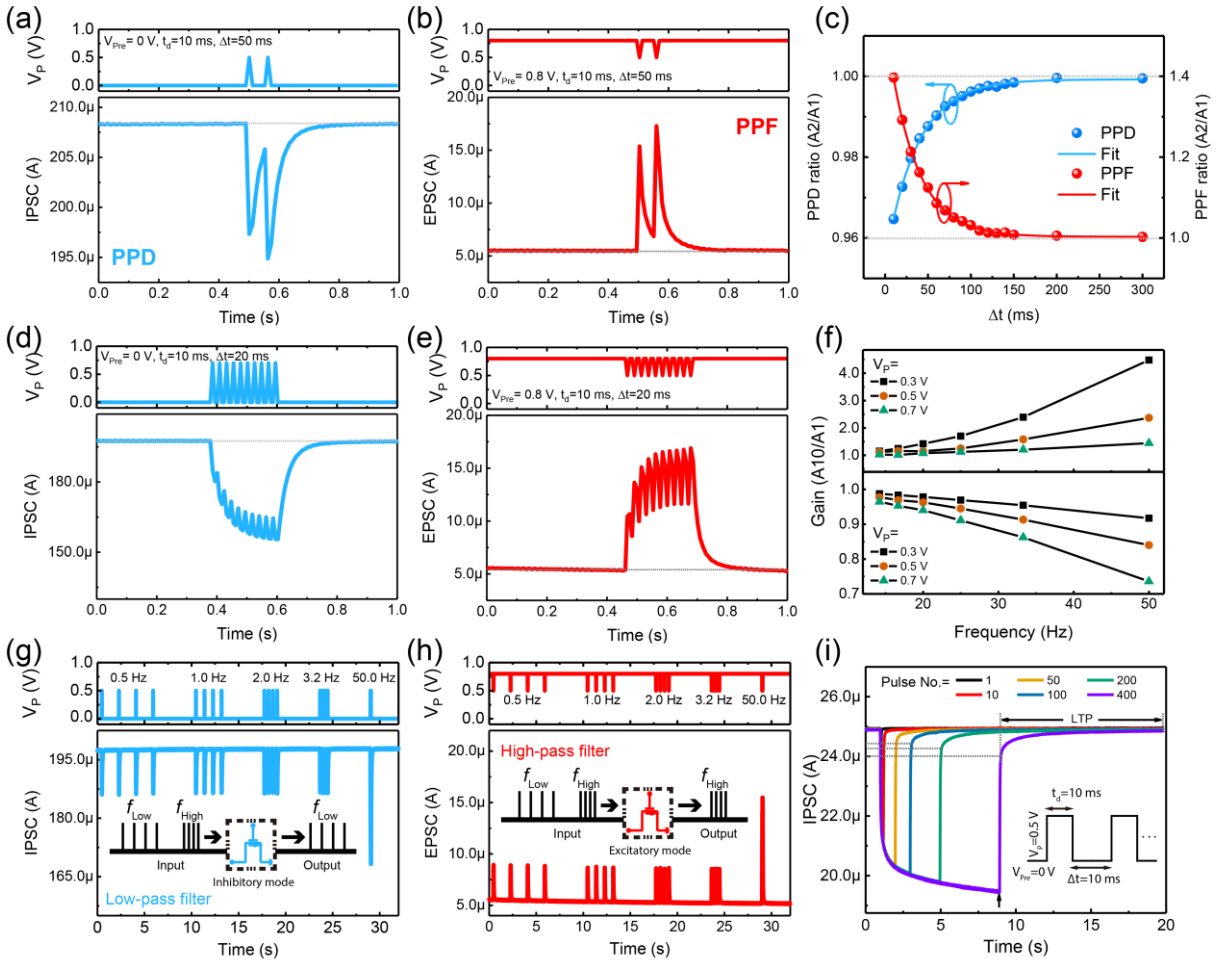

Figure 3. Temporally correlated behaviors. (a) PPD behavior triggered by a pair of pre-synaptic spikes (V_{Pre} = 0 V, V_P = 0.5 V, t_d=10 ms, Δt=50 ms). (b) PPF behavior triggered by a pair of pre-synaptic spikes (V_{Pre} = 0.8 V, V_P = 0.5 V, t_d=10 ms, Δt=50 ms). A1 and A2 represent the absolute peak values of the first and second spike, respectively. (c) PPD and PPF ratio (A2/A1) as a function of spike interval time (Δt). (d) IPSC responses to a stimulus train of 10 presynaptic pulse (V_{Pre} = 0 V, V_P = 0.5 V, t_d=10 ms, Δt=20 ms). (e) EPSC responses to a stimulus train of 10 presynaptic pulse (V_{Pre} = 0.8 V, V_P = 0.5 V, t_d=10 ms, Δt=20 ms). (f) PSC gain (A10/A1) as a function of the presynaptic spike trains with different frequencies (14.2 Hz, 16.7 Hz, 20 Hz, 25 Hz, 33.3 Hz, 50 Hz). Upper panel: excitatory mode at V_{Pre} = 0.8 V. Lower panel: inhibitory mode at V_{Pre} = 0 V. (g) A high-pass temporal filtering function. (h) A low-pass temporal filtering function. (i) IPSCs triggered by different numbers of presynaptic pulses (V_{Pre} = 0 V, V_P = 0.5 V, t_d=10 ms, Δt=10 ms, V_D=0.01 V).

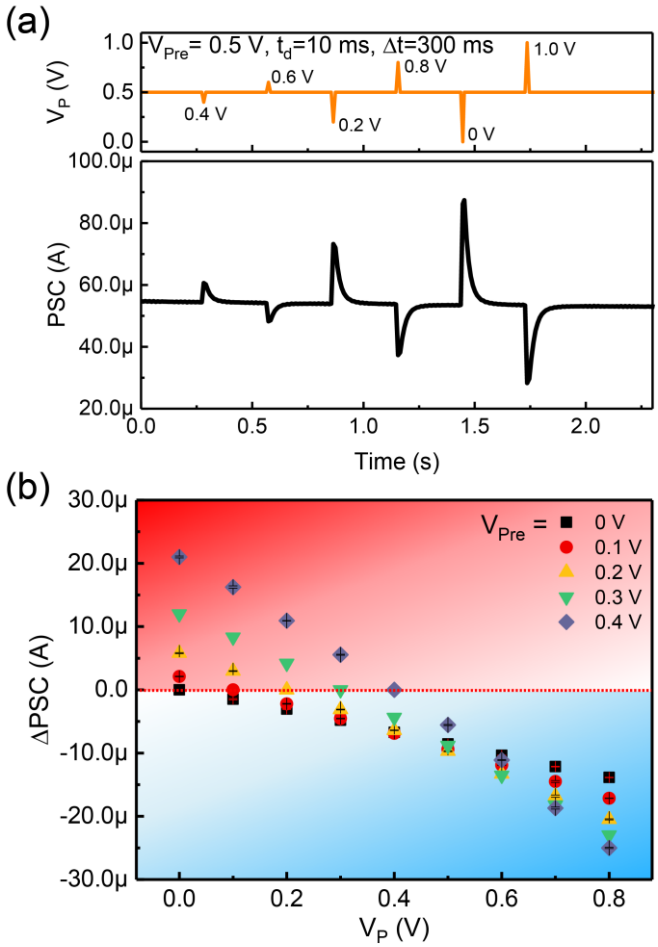

Figure 4. Dynamic reconfiguration of excitatory and inhibitory response modes: (a) Multi-level synapse strength and balanced synaptic strength change obtained through different amplitude of V_P at V_{Pre}= 0.5 V. (b) Synaptic strength changes in response to V_P=0-0.8 V (0.1 V step) at different V_{Pre}=0-0.4 V (0.1 V step).

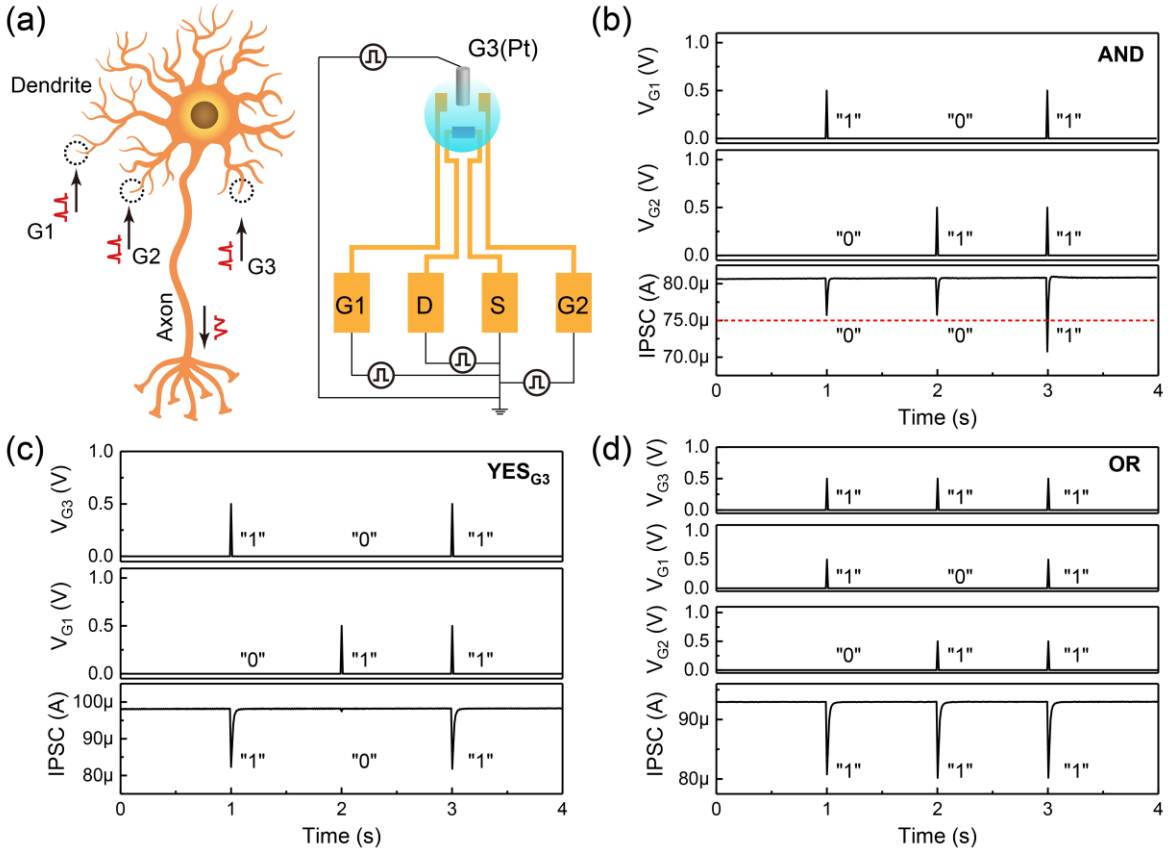

Figure 5. (a) Schematic diagram of the spatial summation with three spatial isolated synapses, and schematic image of the solution-gated OECTs with two in-plane Au (G1, G2) and one Pt (G3) presynaptic inputs (0.5 V, 10 ms). Input–output characteristics of the (b) "AND", (c) "YES_{G3}" and (d) OR logics from the different combinations of presynaptic input terminals. The truth tables are inserted into the corresponding figures.

Dynamically Reconfigurable Short-Term Synapses were demonstrated based on PEDOT:PSS organic electrochemical transistors. The concomitant and independently expressed excitatory and inhibitory plasticity were emulated in a single transistor without additional modulation terminals. Remarkable performances including 10 mV ultrahigh stimulus-resolution and 2 pJ/spike ultralow power consumption were obtained.

Keyword: Artificial synapse, Short-term plasticity, OECTs, Electrochemical doping, Conducting polymer,

Haifeng Ling, Naixiang Wang, Anneng Yang, Yanghui Liu, Jiajun Song and Feng Yan*

Dynamically Reconfigurable Short-Term Synapse with Millivolt Stimulus Resolution Based on Organic Electrochemical Transistors